Tuning Binding of Rubidium Ions to Planar and Curved Negatively Charged π Surfaces

ARTICLE *in* ORGANOMETALLICS · JULY 2013

Impact Factor: 4.13 · DOI: 10.1021/om4001617

6 AUTHORS, INCLUDING:

Sarah N Spisak
University at Albany, The State University of N…
26 PUBLICATIONS **282** CITATIONS
SEE PROFILE

Natalie J Sumner
University at Albany, The State University of N…
8 PUBLICATIONS **51** CITATIONS
SEE PROFILE

Alexander V Zabula
University at Albany, The State University of N…
54 PUBLICATIONS **807** CITATIONS
SEE PROFILE

Andrey Yu Rogachev
Illinois Institute of Technology
78 PUBLICATIONS **641** CITATIONS
SEE PROFILE

ORGANOMETALLICS

Article

pubs.acs.org/Organometallics

Tuning Binding of Rubidium Ions to Planar and Curved Negatively Charged π Surfaces

Sarah N. Spisak,[†] Natalie J. Sumner,[†] Alexander V. Zabula,[†,‡] Alexander S. Filatov,[†] Andrey Yu. Rogachev,[§] and Marina A. Petrukhina*[,†]

[†]Department of Chemistry, University at Albany, State University of New York, Albany, New York 12222, United States

[‡]Department of Chemistry, University of Wisconsin, Madison, Wisconsin 53706-1396, United States

[§]Department of Chemistry and Chemical Biology, Cornell University, Baker Laboratory, Ithaca, New York 14853-1301, United States

Supporting Information

ABSTRACT: Two new rubidium salts of the bowl-shaped corannulene monoanion radical $C_{20}H_{10}^{\bullet-}$ (**1**$^{\bullet-}$), [Rb(15-crown-5)$_2$$^+$][$C_{20}H_{10}^-$] (**2**) and [Rb(dicyclohexano-18-crown-6)$^+$][$C_{20}H_{10}^-$] (**3**), have been synthesized and structurally characterized in this work. An excess of 15-crown-5 ether provided full encapsulation of the rubidium ion in [Rb(15-crown-5)$_2$]$^+$, which precluded metal-directed π interactions with the anionic surface of $C_{20}H_{10}^{\bullet-}$ in the solid-state structure of **2**. The use of more sterically demanding dicyclohexano-18-crown-6 ether prevented the formation of polymeric chains previously seen with 18-crown-6 ether and favored the isolation of the discrete contact ion pair **3**. Complex **3** is built on a convex η^6 coordination of Rb$^+$ to $C_{20}H_{10}^{\bullet-}$, reaffirming the *exo*-binding preference of rubidium ions toward the singly charged corannulene bowl. A rubidium salt of the planar coronene monoanion radical $C_{24}H_{12}^{\bullet-}$ (**4**$^{\bullet-}$), [Rb(18-crown-6)$^+$][$C_{24}H_{12}^-$] (**5**), has also been prepared and structurally characterized to reveal a new binding mode of $C_{24}H_{12}^{\bullet-}$. The analysis of the X-ray structure of **5**, augmented by DFT calculations, confirmed the existence of strong C−H···π interactions between the crown ether and charged surface of $C_{24}H_{12}^{\bullet-}$. These interactions result in a good alignment of matching in size crown ether and coronene moieties, thereby being responsible for the formation of a hub-bound coronene product. DFT calculations were also used to follow the spin density distribution in the [Rb(18-crown-6)][$C_{24}H_{12}$] system as well as in original fragments.

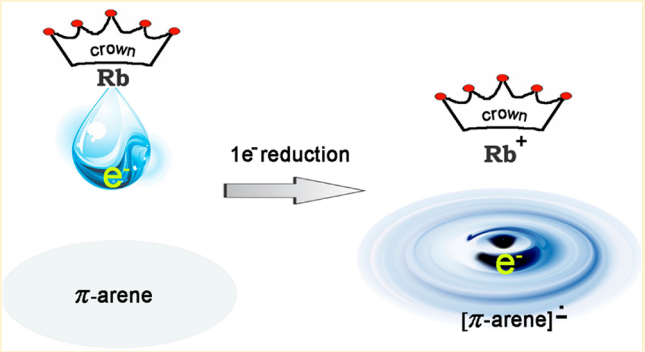

INTRODUCTION

The importance of alkali-metal cation−π interactions relates to their prominence in nature[1] and materials science[2] and thus attracts significant interest from theoretical,[3] experimental,[4] and crystallographic[5] scientific communities. These interests moved over the years from small planar arenes to large and curved polyaromatic systems, ranging from fullerene fragments[6] to fullerenes[7] and nanotubes.[8] We have also contributed to this field and recently accomplished the first structural characterization of alkali-metal salts of mono-,[9] di-,[10] and tetrareduced[11] corannulene, the smallest nonplanar fragment of C_{60}-fullerene. This allowed us to evaluate the binding preferences of Group 1 metals toward the nonplanar π surface of corannulene bearing various negative charges. For the $C_{20}H_{10}^{\bullet-}$ anion, the lightest alkali metals, Li$^+$ and Na$^+$, tend to form solvent-separated ion pairs (SSIP) in the solid state.[9b,10] In contrast, the heavier Rb$^+$ and Cs$^+$ ions prefer to afford contact-ion pairs (CIP) with the $C_{20}H_{10}^{\bullet-}$ bowl, showing a remarkable face selectivity in binding (*exo*-η^6 vs *endo*-η^5, respectively) in the solid products.[9a] However, when the energetics of the above systems are estimated, the DFT calculations[9a] revealed a very small preference (ca. 1.55 kcal mol^{-1}) for Rb$^+$ ions in selecting between the six (η^6)- or five-membered-ring (η^5) sites on the convex surface of $C_{20}H_{10}^{\bullet-}$. This predicted flexibility in binding was also seen experimentally, as two polymorphs of the rubidium salt [Rb(18-crown-6)$^+$][$C_{20}H_{10}^-$] have crystallized under the same experimental conditions.[9a] One exhibited a discrete structure based on η^6 coordination of the Rb$^+$ ion to the benzene ring of $C_{20}H_{10}^{\bullet-}$, while the other formed a 1D polymeric chain with metal binding shifted to the bowl periphery (Scheme 1). After revealing the general binding preferences of Group I metals toward the corannulene monoanion, we now intend to explore how the structure and size variations of macrocyclic crown ethers can be further used for fine tuning of the resulting systems.

RESULTS AND DISCUSSION

Preparation of Corannulene Anions. The acquisition of multiple electrons by corannulene has been extensively studied

Received: February 27, 2013
Published: April 4, 2013

   dx.doi.org/10.1021/om4001617 | *Organometallics* 2013, 32, 3773−3779

Scheme 1. Metal Binding in $[Rb(18\text{-crown-}6)^+][C_{20}H_{10}^-]$

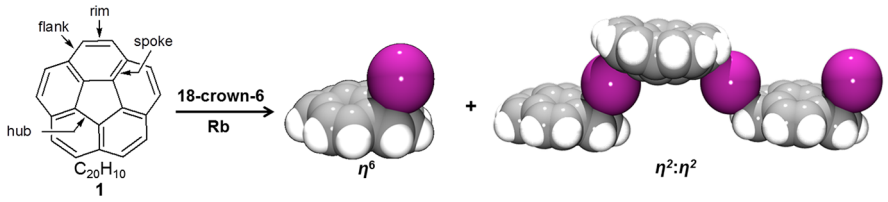

in solution using a combination of spectroscopic tools.[12] The use of lithium metal as a reducing agent is well-known to induce the stepwise reduction of $C_{20}H_{10}$ up to its tetrareduced state.[11−13] In contrast, the reduction processes of corannulene with heavier alkali metals have been less studied. It has been reported that corannulene can be reduced to $C_{20}H_{10}^{4-}$ with rubidium metal over a long period of time, although the exact timing and experimental details were not mentioned.[14] Very broad signals of the resulting tetraanions have been detected in the ^{1}H NMR spectra at low temperatures, indicating possible mixing with a paramagnetic trianion radical.[13b,14]

We observed that addition of rubidium metal to corannulene in THF or DME generates an intense green color associated with the formation of $C_{20}H_{10}^{\bullet-}$, which subsequently undergoes higher reduction to form a deep purple solution. The ease of the second reduction of $C_{20}H_{10}$ makes it hard to practically utilize the first-step reduction for controlled preparation of rubidium salts of monoreduced corannulene. However, we found that reducing $C_{20}H_{10}$ to the dianion stage and adding the appropriate amount of neutral corannulene allows the selective formation of $C_{20}H_{10}^{\bullet-}$ in a controlled fashion (Scheme 2).

Scheme 2. Reduction of $C_{20}H_{10}$ with Rubidium in the Presence of 15-Crown-5 and Dicyclohexano-18-crown-6 (DC18-crown-6) Ethers

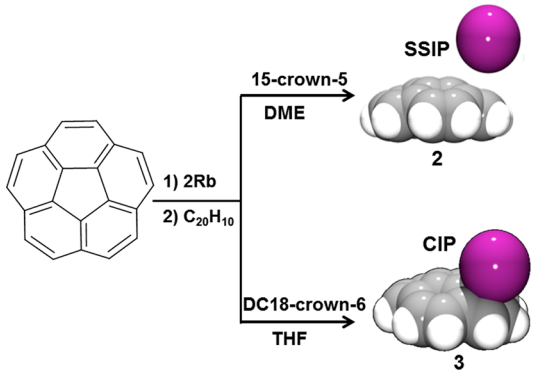

Single crystals of $[Rb(15\text{-crown-}5)_2^+][C_{20}H_{10}^-]\cdot 0.5C_6H_{14}$ ($\mathbf{2}\cdot 0.5C_6H_{14}$) were grown from a DME solution by layering with hexanes. An X-ray diffraction study of $\mathbf{2}\cdot 0.5C_6H_{14}$ (Figure 1a) showed the presence of solvent-separated $C_{20}H_{10}^{\bullet-}$ anions and $[Rb(15\text{-crown-}5)_2]^+$ cations (hexane molecules fill the cavities in the crystal lattice). Notably, this is the first case for the rubidium salts of $C_{20}H_{10}^{\bullet-}$ in which the bowl does not exhibit any direct metal binding.

In **2**, the Rb^+ ion is coordinated by two 15-crown-5 molecules with the corresponding Rb···O bond length distances ranging from 2.84 to 3.17 Å. Overall, the Rb···O interatomic distances are close to those observed in the related compounds.[15] The full encapsulation of Rb^+ centers by ten O atoms of 15-crown-5 ether ligands prevents any interactions

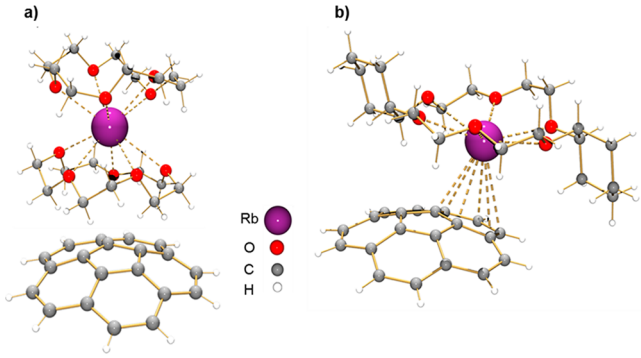

Figure 1. Molecular structures of **2** (a) and **3** (b).

between the alkali-metal ions and the π surface of $C_{20}H_{10}^{\bullet-}$. Previously, "naked" corannulene monoanions have been seen only with light alkali-metal ions such as lithium and sodium.[9b,10]

Crystals of $[Rb(dicyclohexano\text{-}18\text{-crown-}6)^+][C_{20}H_{10}^-]$ (**3**) were grown from THF upon layering with hexanes. In contrast to the case for **2**, an X-ray diffraction study revealed the formation of a contact-ion pair (Figure 1b). The Rb^+ ion is bound to the convex face of the monoanion in an η^6 fashion (Rb···C 3.235(3)−3.572(3) Å). The distance of the Rb center to the benzene ring center (3.14 Å) is indicative of rather strong metal binding to the π bowl. A similar coordination has been seen in the discrete rubidium analogue with 18-crown-6 ether which was found to crystallize along with the 1D product based on the η^2:η^2-bridging mode of $C_{20}H_{10}^{\bullet-}$ (Scheme 1).[9a] The use of bulkier crown ether seems to block the access to the bowl surface for the second metal center, thus preventing the formation of an extended chain, as no polymeric product was found in this case.

Despite the differences in structures **2** and **3**, the changes in the geometry of monoreduced corannulene are quite similar (Table 1). The hub C−C bond lengths of $C_{20}H_{10}^{\bullet-}$ in both cases are close to those measured in neutral corannulene,[16] whereas the spoke and rim C−C bonds are notably elongated. The flank C−C bond lengths of the monoreduced bowl are significantly shortened in comparison to those of the parent molecule. The bowl depths of $C_{20}H_{10}^{\bullet-}$ in **2** and **3**, 0.853(5) and 0.834(4) Å, respectively, are similar to the values seen for the series of corannulene monoanions isolated previously.[9,10] They all show that the acquisition of one electron only slightly reduces the corannulene bowl depth (Table 1). It can be noted that the concave and convex faces of $C_{20}H_{10}^{\bullet-}$ in **2** are engaged in intermolecular C−H···π interactions with the crown moiety of $[Rb(15\text{-crown-}5)_2]^+$, with the shortest contacts found at 2.62 Å. In **3**, the distances between the H atoms of crown ether and the *endo* surface of the bowl start at 2.63 Å.

The ^{1}H NMR spectra of crystals of **2** and **3**, dissolved in THF-d_8, demonstrate low-field shifts for the proton resonances of crown ether moieties (Supporting Information, Figures S1 and S4) in comparison to signals for the respective free crown

dx.doi.org/10.1021/om4001617 | *Organometallics* 2013, 32, 3773−3779

Table 1. Ranges for Key Bond Length Distances, along with the Bowl Depth (Å), for $C_{20}H_{10}$, 2, and 3

	$C_{20}H_{10}$[16b]	2	3[a]
hub	1.411(2)−1.417(2)	1.395(5)−1.422(5)	1.404(4)−1.409(4)
spoke	1.376(2)−1.381(2)	1.398(5)−1.412(5)	1.401(4)−1.411(4)
flank	1.441(2)−1.450(2)	1.410(5)−1.435(5)	1.409(5)−1.442(5)
rim	1.377(2)−1.387(2)	1.409(5)−1.433(6)	1.402(4)−1.430(4)
bowl depth	0.876(2)	0.853(5)	0.834(4)

[a]For the nondisordered corannulene core.

ethers or diamagnetic salts,[17] indicating their interactions with the paramagnetic $C_{20}H_{10}^{\bullet-}$ bowls in solution. Similar low-field shifts of crown protons have been seen for other alkali-metal salts of monoreduced corannulene.[9,10] Furthermore, according to the UV−vis spectra of crystals **2** and **3**, dissolved in DME and THF, respectively (Supporting Information, Figures S2 and S5), the most intense absorbance maxima of $C_{20}H_{10}^{\bullet-}$ are shifted by ca. 15 nm in comparison to those of the in situ generated corannulene monoanions with rubidium ions in THF without crown ethers present.[10a] This may also indicate that some association of the crown ether moieties with monoanions via C−H···π or/and Rb···C interactions exists in solution.

The ESR spectrum of **2** has 11 equally spaced peaks with hyperfine coupling constants (Supporting Information, Figure S3), which is consistent with the ESR signals found at room temperature for the $C_{20}H_{10}^{\bullet-}$ anions with solvent-separated Li^+ or Na^+ ions.[10,12f] The ESR spectrum of **3** (Supporting Information, Figure S6) is more complex than that of **2**. This most probably can be attributed to the coordination of $[Rb(dicyclohexano\text{-}18\text{-}crown\text{-}6)]^+$ to the $C_{20}H_{10}^{\bullet-}$ bowl persisting in the solution of **3**.

Preparation of Coronene Anions. Coronene ($C_{24}H_{12}$, **4**) represents a primary model of a planar π surface of graphene sheets and thus has attracted significant attention from structural and materials chemists.[18−20] Coronene undergoes two phase transitions at 140−180 and 50 K and therefore has only been structurally characterized at ambient temperature.[18,21] A one-electron reduction of coronene has been previously studied with sodium[9b] and potassium[22] metals to yield the solvent-separated ion pair and contact-ion pair in $[Na(DME)_3^+][C_{24}H_{12}^-]$ and $[K(TMEDA)(THF)_2^+][C_{24}H_{12}^-]$, respectively (Scheme 3). Heavier alkali metals have not yet been used as the reducing agents for coronene.

In this work, the reduction of coronene to the monoanion stage was accomplished by the addition of 1.3 equiv of rubidium metal in the presence of 18-crown-6 ether in THF. Single crystals of the product, $[Rb(18\text{-}crown\text{-}6)^+][C_{24}H_{12}^-]$ (**5**), were grown from the THF solution by layering with hexanes. An X-ray diffraction study of **5** revealed the formation of a contact-ion pair with the new binding mode for coronene monoanion (Figure 2).

Scheme 3. Preparation of Alkali-Metal Salts of Monoreduced Coronene $[Na(DME)_3^+][C_{24}H_{12}^-]$[9b] and $[K(TMEDA)(THF)_2^+][C_{24}H_{12}^-]$[22]

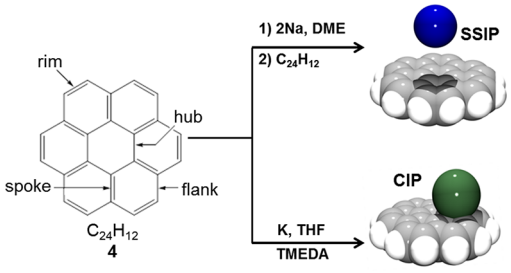

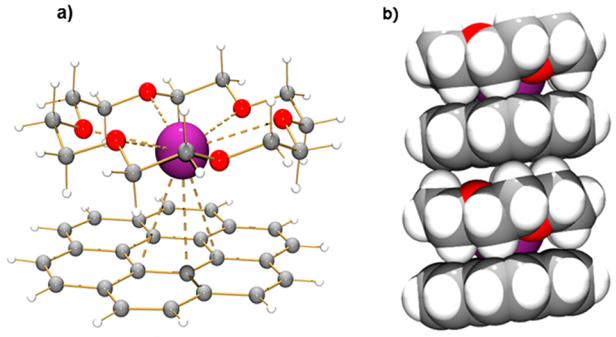

Figure 2. Molecular structure (a) and space-filling depiction of the solid-state packing (b) in **5**.

In **5**, the $[Rb(18\text{-}crown\text{-}6)]^+$ ion is bound to the central benzene ring of $C_{24}H_{12}^{\bullet-}$ with six Rb···C distances (3.312(11), 3.447(10), 3.545(9), 3.685(11), 3.741(11), and 3.968(10) Å) varying broadly. Owing to the large size of rubidium, the ion does not fit inside the cavity of 18-crown-6 ether (the Rb···O bond length distances range from 2.860(8) to 2.996(8) Å) and moves toward the polyarene surface. Notably, this is the first case of a coronene monoanion with a metal bound to the central benzene ring. Previously, the external ring of $C_{24}H_{12}^{\bullet-}$ was engaged in an asymmetric η^6 binding of potassium ions in the structurally characterized $[K(TMEDA)(THF)_2^+][C_{24}H_{12}^-]$ salt.[22,23] Similar to that case, the $C_{24}H_{12}^{\bullet-}$ ligand remains essentially planar in **5**. The hub C−C bond lengths of $C_{24}H_{12}^{\bullet-}$ (average 1.424(13) Å) in the rubidium salt are the same as in neutral $C_{24}H_{12}$ (1.425(3) Å; Table 2).[18] However, the spoke and rim C−C bonds of the monoanion are elongated (average 1.430(13) and 1.371(14) Å vs 1.416(3) and 1.358(3) Å). The flank C−C bond lengths are significantly shortened (average (1.411(15) Å) in comparison to the parent coronene molecule (1.421(3) Å). The C−C bond lengths of the polyarene core in **5** experience the greatest fluctuation upon metal coordination to the hub site in comparison with sodium and potassium salts of monoreduced coronene (Table 2).

In the structure of **5**, the planar surface of $C_{24}H_{12}^{\bullet-}$ is engaged in intermolecular interactions with the crown moiety of $[Rb(18\text{-}crown\text{-}6)]^+$. Intermolecular C−H···$\pi$ contacts as short as 2.84 Å are found in the solid state (Figure 2b). Interestingly, the carbon−oxygen framework of 18-crown-6 ether almost mirrors the disk-like shape of $C_{24}H_{12}^{\bullet-}$. In the solid state, each crown ether molecule is sandwiched between two planar surfaces of coronene radical anions, forming multiple intermolecular C−H···π contacts. Such an alignment of the crown ether and coronene moieties most probably

dx.doi.org/10.1021/om4001617 | Organometallics 2013, 32, 3773−3779

Table 2. Ranges for Key Bond Length Distances (Å) for $C_{24}H_{12}$, 5, $[Na(DME)_3^+][C_{24}H_{12}^-]$, and $[K(TMEDA)(THF)_2^+][C_{24}H_{12}^-]$

	$C_{24}H_{12}$[18]	5	$[Na(DME)_3^+][C_{24}H_{12}^-]$[9b]	$[K(TMEDA)(THF)_2^+][C_{24}H_{12}^-]$[22]
hub	1.425(3)	1.402(14)−1.456(12)	1.418(3)−1.431(3)	1.415(5)−1.434(5)
spoke	1.416(3)	1.407(14)−1.461(13)	1.430(3)−1.441(3)	1.414(4)−1.438(4)
flank	1.421(3)	1.391(15)−1.440(15)	1.396(3)−1.430(4)	1.394(5)−1.424(5)
rim	1.358(3)	1.332(14)−1.390(14)	1.360(4)−1.384(4)	1.366(5)−1.382(5)

directs the Rb^+ ion binding to the central ring of $C_{24}H_{12}^{\bullet-}$, resulting in a coordination mode not seen previously.

The ^1H NMR spectra of crystals **5** dissolved in THF-d_8 (Figure S7, Supporting Information) demonstrate a low-field shift for the crown ether proton resonances, indicating their interaction with the paramagnetic $C_{24}H_{12}^{\bullet-}$ anions in solution. According to the UV−vis spectrum of **5**, dissolved in THF (Figure S8, Supporting Information), the maxima of the two most intense absorption bands of the contact-ion pair in $[Rb(18\text{-crown-}6)^+][C_{24}H_{12}^-]$ (475 and 625 nm) are shifted in comparison to the solvent-separated ion pair in $[Na(DME)_3^+][C_{24}H_{12}^-]$ (478 and 632 nm, DME).[9b]

Theoretical Modeling of the Rb−Coronene System. The unusual binding of Rb^+ ions to the internal ring of $C_{24}H_{12}^{\bullet-}$ in **5** prompted us to perform a comprehensive theoretical investigation of this system. For the first step, two possible coordination sites on the surface of coronene were probed with the simplest model, the "naked" Rb atom. Both isomers (hub and rim, Figure 3a,b) correspond to true minima

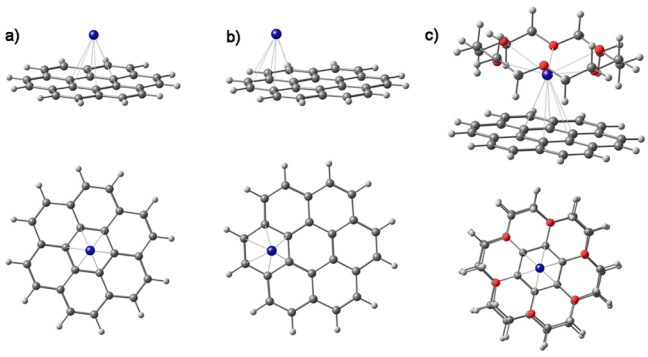

Figure 3. Side and top views for the equilibrium geometry configurations of hub (a) and rim (b) isomers of $[Rb^+][C_{24}H_{12}^-]$ along with $[Rb(18\text{-crown-}6)^+][C_{24}H_{12}^-]$ (c).

on the potential energy surface (PES), as indicated by all-positive Hessian matrices. The energetic difference of 0.2 kcal/mol illustrates that these isomers are indistinguishable in terms of relative stability. Such a degeneracy is also supported by the calculated weak bonding energy between the Rb atom and $C_{24}H_{12}$ surface (−5.23 and −5.47 kcal/mol for the hub and rim isomers, respectively).

To account for the expected contribution from dispersion forces, the recently developed new double-hybrid PBE0-based functional (xDH-PBE0)[24] was applied in single-point calculations for the converged geometry configurations. This provided only a slight increase in bonding energy, and both isomers remained energetically equivalent within ca. 0.5 kcal/mol. Ultimately, we included 18-crown-6 ether into our considerations. Geometry optimization procedures for the rim and hub isomers smoothly converged to the structure where Rb is located at the center of the hub ring (Figure 3c). Careful inspection of the geometry optimization results did not reveal the existence of the rim configuration. Changes in accuracy of numerical calculations did not affect this result. Thus, the hub isomer is found as the only stable geometry configuration for the $[Rb(18\text{-crown-}6)^+][C_{24}H_{12}^-]$ system corresponding to the minimum on the PES.

Subsequent estimations of the bonding energy between $[Rb(18\text{-crown-}6)]$ and $C_{24}H_{12}$ revealed its dramatic increase (−32.47 kcal/mol) in comparison with adducts of unligated Rb with coronene (∼−5.5 kcal/mol). Accounting for dispersion forces in this case added ca. 10 kcal/mol to the total bonding energy (−42.69 kcal/mol). Importantly, the main contribution to the high product stability is provided by C−H···π interactions between the 18-crown-6 ether moiety and the coronene surface. Calculations show the existence of several C−H···C_{rim} contacts within a narrow range of 2.67−2.77 Å.

Electronic Structure of $[Rb(18\text{-crown-}6)][C_{24}H_{12}]$. The system under investigation has an interesting feature—one unpaired electron provided by the rubidium metal. But where is this electron located in the resulting product? Is it fully delocalized over the polyaromatic surface of $C_{24}H_{12}$ or still remains, at least in part, associated with the metal center? To address these questions, we performed a detailed analysis of the electronic structure of $[Rb(18\text{-crown-}6)][C_{24}H_{12}]$ and compared it with that of the "naked" rubidium−coronene model. The charge on the metal center in $[Rb(18\text{-crown-}6)]$ is slightly negative (−0.045e within the NBO formalism),[25] thus being consistent with the electron-donating properties of 18-crown-6 ether. In contrast, in the rubidium adducts with coronene the charge at the metal center becomes highly positive (+0.849e in $[Rb(18\text{-crown-}6)][C_{24}H_{12}]$ and +0.986e in both isomers of $[Rb][C_{24}H_{12}]$). This formally indicates almost a full one-electron transfer from the metal to a polyarene to form the contact-ion pair $[Rb(18\text{-crown-}6)^+][C_{24}H_{12}^-]$ or $[Rb^+][C_{24}H_{12}^-]$. Interestingly, an analysis of distribution of spin density function (Figure 4, left) shows that the unpaired electron in $[Rb(18\text{-crown-}6)]$ is *not* localized on the rubidium center but is being pushed out to the side opposite to the bound crown ether ligand.

This observation fully agrees with the atomic spin density on Rb center, which is 0 for $[Rb(18\text{-crown-}6)]$. At the same time, in the $[Rb(18\text{-crown-}6)^+][C_{24}H_{12}^-]$ adduct the spin density is found to be delocalized over the π surface of the coronene (Figure 4, center). Thus, the formation of a contact-ion pair can be described as a falling drop of spin density (here corresponds to one unpaired electron) from $[Rb(18\text{-crown-}6)]$ to the coronene surface. The localization of spin density outside the metal center explains the relative ease of electron transfer to the polyaromatic system. The spin density distribution in $[Rb(18\text{-crown-}6)^+][C_{24}H_{12}^-]$ coincides precisely with the topology of the LUMO of neutral $C_{24}H_{12}$ (Figure 4, right). It fully supports the conclusion regarding the formation of $C_{24}H_{12}^{\bullet-}$ and the closed-shell Rb^+ cation in this system.

dx.doi.org/10.1021/om4001617 | *Organometallics* 2013, 32, 3773−3779

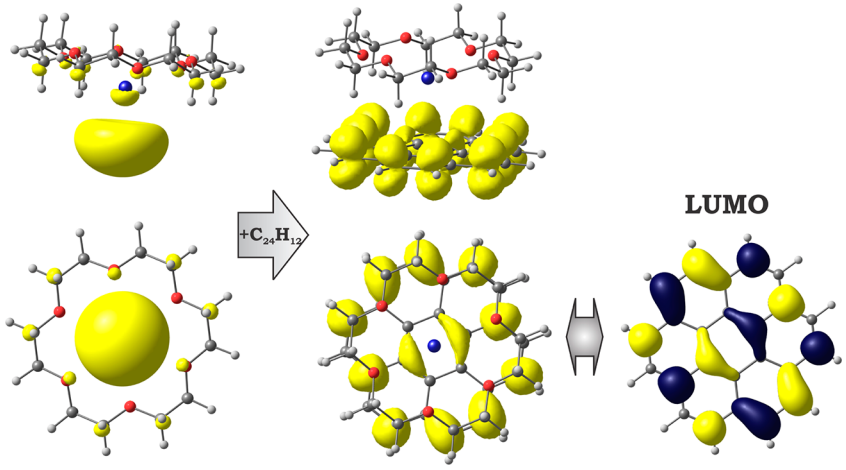

Figure 4. Spin density distribution in [Rb(18-crown-6)] (left) and [Rb(18-crown-6)$^+$][$C_{24}H_{12}^-$] (center): (top) side views; (bottom) top views. The topology of LUMO of $C_{24}H_{12}$ is also shown for comparison (right).

CONCLUSIONS

Interactions of alkali-metal ions with extended π systems are generally weak and can be affected by a variety of additional factors. In this work, we have shown that the size and substitution variations built into the crown ether structures permit us to finely tune the alkali-metal binding toward the charged π surfaces of corannulene and coronene. For example, $Rb^+-\pi$ interactions can be completely excluded by providing full metal ion encapsulation through an excess of small 15-crown-5 ether. In contrast, the use of the larger and bulkier dicyclohexano-18-crown-6 ether favors the formation of a contact-ion pair based on a η^6-convex coordination of Rb^+ to the $C_{20}H_{10}^{\bullet-}$ bowl. A new hub coordination mode is found in the rubidium salt of the coronene monoanion radical in the presence of 18-crown-6 ether. This type of binding most probably results from a good size match of two building units, allowing them to fully maximize C−H···π interactions upon their perfect overlap, as shown by X-ray crystallography and DFT calculations.

EXPERIMENTAL SECTION

Materials and Methods. All manipulations were carried out using break-and-seal[26] and glovebox techniques under an atmosphere of argon. Solvents (THF and hexanes) were dried over Na/benzophenone and distilled prior to use. THF-d_8 and DME were dried over NaK_2 alloy and vacuum-transferred. The crown ethers, 15-crown-5 and 18-crown-6, were purchased from Strem Chemicals. Dicyclohexano-18-crown-6 was purchased from Sigma Aldrich. All crown ethers were dried over P_2O_5 in vacuo for 24 h. Rubidium metal was purchased from Strem Chemicals. Corannulene was prepared as described previously[27] and sublimed at 175 °C prior to use. Coronene was purchased from TCI America and sublimed at 240 °C prior to use. The ^{1}H NMR spectra were measured on a Bruker AC-400 spectrometer at 400 MHz and were referenced to the resonances of the corresponding solvent used. The ESR spectra were recorded on a Bruker ER-200 D-SRC X-band spectrometer that is interfaced to a Compaq 386 PC equipped with the IBM analog-to-digital converter and Scientific Software Services Systems (Bloomington, IL). The UV−vis spectrum of **2** was recorded on a PerkinElmer Lambda 35 spectrometer. The UV−vis spectra of **3** and **5** were recorded on a Thermo Scientific Evolution 300BB spectrometer. Elemental analyses were performed by Complete Analysis Laboratories, Inc., Parsippany, NJ.

Preparation of [Rb(15-crown-5)$_2^+$][$C_{20}H_{10}^-$] (2). DME (3 mL) was added to a flask containing Rb metal (10 mg, 0.12 mmol), corannulene (10 mg, 0.04 mmol), and 15-crown-5 ether (44 mg, 0.20 mmol). The resulting deep green solution was stirred at room temperature for 12 h to give the bright purple corannulene dianion. The mixture was filtered and combined with a solution of neutral corannulene (10 mg, 0.04 mmol) in DME (2 mL). Hexanes (3 mL) was added to the resulting green solution, and the mixture was kept at 10 °C. The green crystalline precipitate was collected in 24 h, washed several times with hexanes, and dried in vacuo. Yield: 46 mg, 74%. ^{1}H NMR (400 MHz, THF-d_8, 25 °C, ppm): δ 4.41 (OCH_2, 15-crown-5). UV−vis (DME, nm): λ_{max} 662.

To access X-ray-quality crystals, the above green solution was carefully layered with hexanes (3 mL) and kept at 10 °C. Cube-shaped green crystals, **2**·0.5C_6H_{14}, were collected in 48 h. Yield: 34 mg, 53%.

Preparation of [Rb(dicyclohexano-18-crown-6)$^+$][$C_{20}H_{10}^-$] (3). THF (3 mL) was added to a flask containing Rb metal (10 mg, 0.12 mmol), corannulene (10 mg, 0.04 mmol), and dicyclohexano-18-crown-6 ether (31 mg, 0.083 mmol). The resulting deep green solution was stirred at room temperature for 12 h to give the bright purple corannulene dianion. The mixture was filtered and combined with a solution of neutral corannulene (10 mg, 0.04 mmol) in THF (2 mL). The resulting green solution was layered with hexanes (3 mL) and kept at 10 °C. The X-ray-quality block-shaped crystals of **3** were collected in 56 h. Yield: 34 mg, 60%. Anal. Calcd for $C_{40}H_{46}RbO_6$: C, 67.83; H, 6.55. Found: C, 67.36; H, 6.19. UV−vis (THF, nm): λ_{max} 661.

Preparation of [Rb(18-crown-6)$^+$][$C_{24}H_{12}^-$] (5). THF (3 mL) was added to a flask containing Rb metal (3.7 mg, 0.043 mmol, 1.3 equiv), 18-crown-6 ether (15.8 mg, 0.06 mmol), and coronene (10 mg, 0.033 mmol). The initially green solution was stirred at room temperature for 8 h to produce a deep green mixture. The mixture was filtered, layered with hexanes (3 mL), and kept at 10 °C. X-ray-quality block-shaped crystals of **5** were collected in 48 h. Yield: 14 mg, 65%. Anal. Calcd for $C_{36}H_{36}RbO_6$: C, 66.51; H, 5.58. Found: C, 66.44; H, 5.49. ^{1}H NMR (400 MHz, THF-d_8, 25 °C, ppm): δ 4.78 (OCH_2, 18-crown-6).

Crystal Structure Determinations and Refinement. Data collections were performed on a Bruker SMART APEX CCD-based X-ray diffractometer with graphite-monochromated Mo Kα radiation (λ = 0.71073 Å) at T = 100(2) K. Data were corrected for absorption effects using the empirical method SADABS.[28] The structures were solved by direct methods and refined using the Bruker SHELXTL (version 6.14) software package.[29] All atoms were refined with anisotropic parameters. Hydrogen atoms were included at idealized positions using the riding model. In **3**, the crown ether ligands are rotationally disordered over two positions, and this disorder was modeled with a 0.6:0.4 ratio of two parts. In **5**, the Rb center is disordered over two positions, and this disorder was modeled with a

dx.doi.org/10.1021/om4001617 | Organometallics 2013, 32, 3773−3779

0.57:0.43 ratio of two parts. For further crystal and data collection details see Table S1 in the Supporting Information.

Calculation Details. Geometry optimizations were performed at the DFT level of theory with help of the hybrid exchange-correlation functional PBE0.[30] The rubidium atom was described by the def2-TZVP basis set in conjunction with a Stuttgart–Bonn effective core potential. Atoms of organic ligands (C, H, O) were described by cc-pVDZ basis sets. All calculated structures correspond to local minima (no imaginary frequencies) on the corresponding potential energy surfaces, as determined by calculation of the full Hessian matrix followed by estimation of frequencies in the harmonic approximation. The expected influence of dispersion forces was accounted for by applying the newly developed double-hybrid functional xDH-PBE0,[24] originally based on the PBE0 hybrid functional. These single-point calculations were performed for converged geometries by using the same atomic basis sets. All calculations were carried out by using the Firefly program package (version 8.0.0 beta).[31]

Optimized geometries were used to get an insight into the electronic structure of target systems in terms of natural bond orbitals (NBO).[25] All computations were performed with the GENNBO (version 5.0) program,[32] using the converged wave functions generated by the Firefly program. Molecular orbital and spin density pictures were created by the ChemCraft program.[33]

■ ASSOCIATED CONTENT

Ⓢ Supporting Information

Figures and CIF files giving ESR, UV–vis, and NMR spectra and crystallographic data of **2**, **3**, and **5**. This material is available free of charge via the Internet at http://pubs.acs.org. CCDC 918809–918811 also contain supplementary crystallographic data for **2**, **3**, and **5**. These data can be obtained free of charge from the Cambridge Crystallographic Data Centre via www.ccdc.cam.ac.uk/data_request/cif.

■ AUTHOR INFORMATION

Corresponding Author

*M.A.P.: e-mail, mpetrukhina@albany.edu; fax, +1 518 442 3462; tel, +1 518 442 4406.

Notes

The authors declare no competing financial interest.

■ ACKNOWLEDGMENTS

Financial support of this work from the National Science Foundation Award (CHE-1212441) is gratefully acknowledged. We thank the University at Albany for supporting the X-ray Center at the Department of Chemistry, Dr. V. M. Grigoryants for recording the ESR spectra, and Dr. A. A. Granovsky and the Firefly team for providing a developing version of the Firefly program package. S.N.S. also thanks the International Centre for Diffraction Data (ICDD) for the 2012 and 2013 Ludo Frevel Crystallography Scholarship.

■ REFERENCES

(1) (a) Page, M. J.; Cera, E. D. *Physiol. Rev.* **2006**, *86*, 1049–1092. (b) Dougherty, D. A. *Science* **1996**, *271*, 163–168.

(2) (a) Zhang, C.; Gamble, S.; Ainsworth, D.; Slawin, A. M. Z.; Andreev, Y. G.; Bruce, P. G. *Nat. Mater.* **2009**, *8*, 580–584. (b) Mitsuhashi, R.; Suzuki, Y.; Yamanari, Y.; Mitamura, H.; Kambe, T.; Ikeda, N.; Okamoto, H.; Fujiwara, A.; Yamaji, M.; Kawasaki, N.; Maniwa, Y.; Kubozono, Y. *Nature* **2010**, *464*, 76–79. (c) Kubozono, Y.; Mitamura, H.; Lee, X.; He, X.; Yamanari, Y.; Takahashi, Y.; Suzuki, Y.; Kaji, Y.; Eguchi, R.; Akaike, K.; Kambe, T.; Okamoto, H.; Fujiwara, A.; Kato, T.; Kosugi, T.; Aoki, H. *Phys. Chem. Chem. Phys.* **2011**, *13*, 16476–16493. (d) Xue, M.; Cao, T.; Wang, D.; Wu, Y.; Yang, H.; Dong, X.; He, J.; Li, F.; Chen, G. F. *Sci. Rep.* **2012**, *2*, 1–4. (e) Mahadevi, A. S.; Sastry, G. N. *Chem. Rev.* **2013**, *113*, 2100–2138 and references therein.

(3) (a) Froudakis, G. E. *Nano Lett.* **2001**, *1*, 531–533. (b) Ilkhechi, A. H.; Mercero, J. M.; Silanes, I.; Bolte, M.; Scheibitz, M.; Lerner, H.-W.; Ugalde, J. M.; Wagner, M. *J. Am. Chem. Soc.* **2005**, *127*, 10656–10666. (c) Mpourmpakis, G.; Tylianakis, E.; Papanikolaou, D.; Froudakis, G. *Rev. Adv. Mater. Sci.* **2006**, *11*, 92–97. (d) Coletti, C.; Re, N. *J. Phys. Chem. A* **2006**, *110*, 6563–6570. (e) Zheng, X.; Wang, X.; Yi, S.; Wang, N.; Peng, Y. *J. Comput. Chem.* **2010**, *31*, 1458–1468. (f) Zurek, E. *J. Am. Chem. Soc.* **2011**, *133*, 4829–4839. (g) Green, J. R.; Dunbar, R. C. *J. Phys. Chem. A* **2011**, *115*, 4968–4979.

(4) (a) Ma, J. C.; Dougherty, D. A. *Chem. Rev.* **1997**, *97*, 1303–1324. (b) Smith, J. D. *Adv. Organomet. Chem.* **1998**, *43*, 267–348. (c) Gokel, G. W.; Barbour, L. J.; De Wall, S. L.; Meadows, E. S. *Coord. Chem. Rev.* **2001**, *22*, 127–154. (d) Christy, F. A.; Shrivastav, P. S. *Crit. Rev. Anal. Chem.* **2011**, *41*, 236–269. (e) Zabula, A. V.; Sumner, N. J.; Filatov, A. S.; Spisak, S. N.; Grigoryants, V. M.; Petrukhina, M. A. *Eur. J. Inorg. Chem.* **2012**, 4675–4683.

(5) (a) Hubig, S. M.; Lindeman, S. V.; Kochi, J. K. *Coord. Chem. Rev.* **2000**, *200*, 831–873. (b) Steed, J. W. *Coord. Chem. Rev.* **2001**, *215*, 171–221. (c) Fukin, G. K.; Lindeman, S. V.; Kochi, J. K. *J. Am. Chem. Soc.* **2002**, *124*, 8329–8336. (d) Gorrell, I. B. *Annu. Rep. Prog. Chem. A* **2003**, *99*, 3–19.

(6) (a) Filatov, A. S.; Petrukhina, M. A. *Coord. Chem. Rev.* **2010**, *254*, 2234–2246. (b) Filatov, A. S.; Scott, L. T.; Petrukhina, M. A. *Cryst. Growth Des.* **2010**, *10*, 4607–4621. (c) *Fragments of Fullerenes and Carbon Nanotubes: Designed Synthesis, Unusual Reactions, and Coordination Chemistry*; Petrukhina, M. A., Scott, L. T., Eds.; Wiley: Hoboken, NJ, 2012.

(7) (a) Matsuo, Y.; Nakamura, E. Application of Fullerenes to Nanodevices. In *Chemistry of Nanocarbons*; Akasaka, T., Wudl, F., Nagase, S., Eds., Wiley: Chichester, U.K., 2010; pp 173–187. (b) Rodríguez-Fortea, A.; Balch, A. L.; Poblet, J. M. *Chem. Soc. Rev.* **2011**, *40*, 3551–3563. (c) Lu, X.; Akasaka, T.; Nagase, S. *Chem. Commun.* **2011**, *47*, 5942–5957.

(8) (a) Chamberlain, T. W.; Meyer, J. C.; Biskupek, J.; Leschner, J.; Santana, A.; Besley, N. A.; Bichoutskaia, E.; Kaiser, U.; Khlobystov, A. N. *Nat. Chem.* **2011**, *3*, 732–737. (b) Giménez-López, M. C.; Moro, F.; La Torre, A.; Gómez-García, C. J.; Brown, P. D.; van Slageren, J.; Khlobystov, A. N. *Nat. Commun.* **2011**, *2*, 1415/1–1415/6.

(9) (a) Spisak, S. N.; Zabula, A. V.; Filatov, A. S.; Rogachev, A. Yu.; Petrukhina, M. A. *Angew. Chem., Int. Ed.* **2011**, *50*, 8090–8094. (b) Filatov, A. S.; Sumner, N. J.; Spisak, S. N.; Zabula, A. V.; Rogachev, A. Yu.; Petrukhina, M. A. *Chem. Eur. J.* **2012**, *18*, 15753–15760.

(10) (a) Zabula, A. V.; Spisak, S. N.; Filatov, A. S.; Grigoryants, V. M.; Petrukhina, M. A. *Chem. Eur. J.* **2012**, *18*, 6476–6484. (b) Spisak, S. N.; Zabula, A. V.; Ferguson, M. V.; Filatov, A. S.; Petrukhina, M. A. *Organometallics* **2013**, *32*, 538–543.

(11) (a) Zabula, A. V.; Filatov, A. S.; Spisak, S. N.; Rogachev, A. Yu.; Petrukhina, M. A. *Science* **2011**, *333*, 1008–1011. (b) Zabula, A. V.; Spisak, S. N.; Filatov, A. S.; Petrukhina, M. A. *Organometallics* **2012**, *31*, 5541–5545. (c) Zabula, A. V.; Spisak, S. N.; Filatov, A. S.; Petrukhina, M. A. *Angew. Chem., Int. Ed.* **2012**, *51*, 12194–12198.

(12) (a) Ayalon, A.; Sygula, A.; Cheng, P.-C.; Rabinovitz, M.; Rabideau, P. W.; Scott, L. T. *Science* **1994**, *265*, 1065–1067. (b) Baumgarten, M.; Gherghel, J. L.; Wagner, M.; Weitz, A.; Rabinovitz, M.; Cheng, P.-C.; Scott, L. T. *J. Am. Chem. Soc.* **1995**, *117*, 6254–6257. (c) Weitz, A.; Rabinovitz, M.; Cheng, P.-C.; Scott, L. T. *Synth. Met.* **1997**, *86*, 2159–2160. (d) Weitz, A.; Shabtai, E.; Rabinovitz, M.; Bratcher, M. S.; McComas, C. C.; Best, M. D.; Scott, L. T. *Chem. Eur. J.* **1998**, *4*, 234–239. (e) Shenhar, R.; Willner, I.; Preda, D. V.; Scott, L. T.; Rabinovitz, M. *J. Phys. Chem. A* **2000**, *104*, 10631–10636. (f) Sato, T.; Yamamoto, A.; Tanaka, H. *Chem. Phys. Lett.* **2000**, *326*, 573–579. (g) Aprahamian, I.; Eisenberg, D.; Hoffman, R. E.; Sternfeld, T.; Matsuo, Y.; Jackson, E. A.; Nakamura, E.; Scott, L. T.; Sheradsky, T.; Rabinovitz, M. *J. Am. Chem. Soc.* **2005**, *127*, 9581–9587. (h) Aprahamian, I.; Wegner, H. A.; Sternfeld, T.; Rauch, K.; de Meijere, A.; Sheradsky, T.; Scott, L. T.; Rabinovitz, M. *Chem. Asian J.* **2006**, *1*, 678–685. (i) Treitel, N.; Sheradsky, T.; Peng, L.; Scott, L. T.;

Rabinovitz, M. *Angew. Chem., Int. Ed.* **2006**, *45*, 3273−3277. (j) Eisenberg, D.; Quimby, J. M.; Jackson, E. A.; Scott, L. T.; Shenhar, R. *Chem. Commun.* **2010**, *46*, 9010−9012. (k) Eisenberg, D.; Shenhar, R. *WIREs Comput. Mol. Sci.* **2012**, *2*, 525−547.
(13) (a) Ayalon, A.; Rabinovitz, M.; Cheng, P.-C.; Scott, L. T. *Angew. Chem., Int. Ed. Engl.* **1992**, *31*, 1636−1637. (b) Shabtai, E.; Hoffman, R. E.; Cheng, P.-C.; Bayrd, E.; Preda, D. V.; Scott, L. T.; Rabinovitz, M. *J. Chem. Soc., Perkin Trans. 2* **1999**, 129−133.
(14) Aprahamian, I.; Preda, D. V.; Bancu, M.; Belanger, A. P.; Sheradsky, T.; Scott, L. T.; Rabinovitz, M. *J. Org. Chem.* **2006**, *71*, 290−298.
(15) (a) Neander, S.; Behrens, U.; Olbrich, F. *J. Organomet. Chem.* **2000**, *604*, 59−67. (b) Boeddinghaus, M. B.; Wahl, B.; Fässler, T. F.; Jakes, P.; Eichel, R.-A. *Z. Anorg. Allg. Chem.* **2012**, *638*, 2205−2212.
(16) (a) Hanson, J. C.; Nordman, C. E. *Acta Crystallogr., Sect. B* **1976**, *32*, 1147−1153. (b) Petrukhina, M. A.; Andreini, K. W.; Mack, J.; Scott, L. T. *J. Org. Chem.* **2005**, *70*, 5713−5716.
(17) Kähler, T.; Behrens, U.; Neander, S.; Olbrich, F. *J. Organomet. Chem.* **2002**, *649*, 50−54.
(18) (a) Robertson, J. M.; White, J. G. *Nature* **1944**, *154*, 605−606. (b) Robertson, J. M.; White, J. G. *J. Chem. Soc.* **1945**, 607−617. (c) Krygowski, T. M.; Cyranski, M.; Ciesielski, A.; Swirska, B.; Leszcynski, P. *J. Chem. Inf. Comput. Sci.* **1996**, *36*, 1135−1141.
(19) (a) Scanlon, L. G.; Sandi, G. *J. Power Sources* **1999**, *81*−*82*, 176−181. (b) Ruuska, H.; Pakkanen, T. A. *J. Phys. Chem.* **2001**, *105*, 9541−9547. (c) Kubozono, Y.; Mitamura, H.; Lee, X.-S.; He, X.-X.; Yamanari, Y.; Takahashi, Y.; Suzuki, Y.; Kaji, Y.; Eguchi, R.; Akaike, K.; Kambe, T.; Okamoto, H.; Fujiwara, A.; Kato, T.; Kosugi, T.-I.; Aoki, H. *Phys. Chem. Chem. Phys.* **2011**, *13*, 16476−16493. (d) Okazaki, T.; Iizumi, Y.; Okubo, S.; Kataura, H.; Liu, Z.; Suenaga, K.; Tahara, Y.; Yudasaka, M.; Okada, S.; Iijima, S. *Angew. Chem., Int. Ed.* **2011**, *50*, 4853−4857.
(20) Gross, L.; Mohn, F.; Moll, N.; Schuler, B.; Criado, A.; Guitian, E.; Pena, D.; Gourdon, A.; Meyer, G. *Science* **2012**, *337*, 1326−1329.
(21) Yamamoto, T.; Nakatani, S.; Nakamura, T.; Mizuno, K.; Matsui, A. H.; Akahama, Y.; Kawamura, H. *Chem. Phys.* **1994**, *184*, 247−254.
(22) Janiak, C.; Hemling, H. *Chem. Ber* **1994**, *127*, 1251−1253.
(23) For a complex of neutral coronene with the $\{Rh(PiBu_3)_2\}^+$ fragment, see: Woolf, A.; Chaplin, A. B.; McGrady, J. E.; Alibadi, M. A. M.; Rees, N.; Draper, S.; Murphy, F.; Weller, A. S. *Eur. J. Inorg. Chem.* **2011**, 1614−1625.
(24) Zhang, I. Y.; Su, N. Q.; Brémond, E. A. G.; Adamo, C.; Xu, X. *J. Chem. Phys.* **2012**, *136*, 174103−1−174103−8.
(25) (a) Weinhold, F.; Landis, C. A. *Valency and Bonding: A Natural Bond Orbital Donor−Acceptor Perspective*; Cambridge University Press: Cambridge, U.K., 2005. (b) Reed, A. E.; Curtiss, L. A.; Weinhold, F. *Chem. Rev.* **1988**, *88*, 899−926.
(26) Kozhemyakina, N. V.; Nuss, J.; Jansen, M. *Z. Anorg. Allg. Chem.* **2009**, *635*, 1355−1361.
(27) (a) Mehta, G.; Panda, G. *Tetrahedron Lett.* **1997**, *38*, 2145−2148. (b) Scott, L. T.; Cheng, P.-C.; Hashemi, M. M.; Bratcher, M. S.; Meyer, D. T.; Warren, H. B. *J. Am. Chem. Soc.* **1997**, *119*, 10963−10968. (c) Sygula, A.; Xu, G.; Marcinow, Z.; Rabideau, P. W. *Tetrahedron* **2001**, *57*, 3637−3644.
(28) *SADABS*; Bruker AXS, Madison, WI, 2001.
(29) (a) Sheldrick, G. M. *Acta Crystallogr.* **2008**, *A64*, 112−122. (b) *SHELXTL,Version 6.14*; Bruker AXS, Madison, WI, 2000.
(30) (a) Perdew, J. P.; Burke, K.; Ernzerhof, M. *Phys. Rev. Lett.* **1996**, *77*, 3865−3868. (b) Perdew, J. P.; Burke, K.; Ernzerhof, M. *Phys. Rev. Lett.* **1997**, *78*, 1396.
(31) Granovsky, A. A. *Firefly, v.7.1.G*; http://classic.chem.msu.su/gran/gamess/index.html.
(32) Glendening, E. D.; Badenhoop, J. K.; Reed, A. E.; Carpenter, J. E.; Bohmann, J. A.; Morales, C. A.; Weinhold, F. *NBO 5.0*; University of Wisconsin, Madison, WI, 2001.
(33) Zhurko, G. A. *ChemCraft*; http://www.chemcraftprog.com.